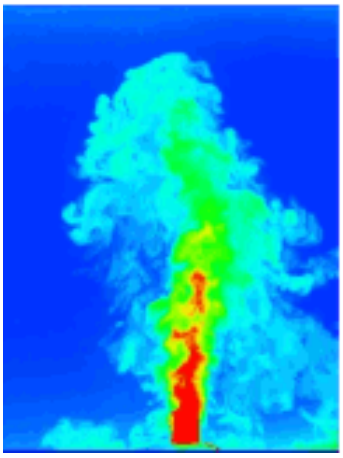

Journal of Turbulence
Publication details, including instructions for authors and subscription information:
http://www.informaworld.com/smpp/title~content=t713665472

Can the dynamic eddy-viscosity class of subgrid-scale models capture inertial-range properties of Burgers turbulence?

Sukanta Basu [a]
[a] Atmospheric Science Group, Department of Geosciences, Texas Tech University, Lubbock, TX, USA

First Published on: 01 January 2009

To cite this Article Basu, Sukanta(2009)'Can the dynamic eddy-viscosity class of subgrid-scale models capture inertial-range properties of Burgers turbulence?',Journal of Turbulence, Volume 10, Art. No. N12,
To link to this Article: DOI: 10.1080/14685240902852719
URL: http://dx.doi.org/10.1080/14685240902852719

Journal of Turbulence
Vol. 10, No. 12, 2009, 1–16

Taylor & Francis
Taylor & Francis Group

Can the dynamic eddy-viscosity class of subgrid-scale models capture inertial-range properties of Burgers turbulence?

Sukanta Basu*

Atmospheric Science Group, Department of Geosciences, Texas Tech University, Lubbock, TX 79409, USA

(*Received 30 October 2008; final version received 12 February 2009*)

The one-dimensional stochastic Burgers equation has the remarkable ability to mimic some of the fundamental statistical and dynamical properties of three-dimensional fully developed turbulence. In this study, we numerically investigate the competence of commonly used dynamic eddy-viscosity-type subgrid-scales (SGSs) models in large-eddy simulation of this equation. We found that the inertial-range characteristics of Burgers turbulence (also known as Burgulence) are well preserved by this class of SGS models.

Keywords: Burgers equation; large-eddy simulation; multifractal; subgrid scale

1. Introduction

Large-eddy simulation (LES) is at present the most efficient technique available for high-Reynolds-number turbulent flow simulations, in which the larger scales of motion are explicitly resolved and in which the smaller ones subgridscales, SGSs are parameterized. Due to strong influence of the SGS parameterization on the dynamics of the resolved turbulence, considerable research efforts have been made during the past decades, and several SGS models have been proposed (see [1–4] for recent reviews). Without any doubt, the dynamic eddy-viscosity SGS models [5, 6] and their modified versions are the most widely used SGS models. These models proved to be very successful in various LES applications [7]. However, it is not known whether this class of SGS models can capture essential inertial-range characteristics (e.g., multifractality) of high-Reynolds-number turbulence. In order to answer this question conclusively, one would need to perform three-dimensional direct numerical simulation (DNS) of high-Reynolds-number turbulent flows and subsequently compare the higher-order statistics derived from the filtered DNS fields with the LES-generated statistics. Unfortunately, such a task is computationally prohibitive at the present time. For this reason, in the present paper, we address this intriguing question using the one-dimensional stochastic (multifractal) Burgers equation as a testbed.

Burgers equation [8] and its stochastic variants have been often used in the literature either to gain insight into complex structure of fully developed three-dimensional turbulence or to validate a new methodology before generalizing it to the three-dimensional case (see [9–13] for SGS modeling; [14] for Karhunen–Loéve expansion of turbulent flows; [15] for feedback control, among others). Apart from simplicity, the popularity of Burgers equation

*Email: sukanta.basu@ttu.edu

ISSN: 1468-5248 online only

DOI: 10.1080/14685240902852719
http://www.informaworld.com

could be attributed to its apparent similarity to three-dimensional turbulence (e.g., nonlinearity structure, energy spectrum, intermittency of energy dissipation) and ease of numerical computation. At the same time, this equation has also been a favorite toy model for turbulence in the theoretical physics community because of its analytical tractability [16–30].

The organization of this paper is as follows: In the following section, we describe the DNS of the stochastic Burgers equation (SBE) and compare it with published theoretical and numerical results. Then, in Section 3, we proceed with the description of the LES results, using two commonly used dynamic eddy-viscosity SGS models.[1] The simulated results are compared in detail with the filtered DNS results. A comprehensive set of statistics (e.g., kinetic energy, SGS energy dissipation, enstrophy balance, higher-order moments, temporal decorrelation) are considered in order to draw inferences on the accuracy of dynamic SGS modeling approach in the present context. Conclusions are presented in Section 4.

2. DNS of the SBE

The one-dimensional SBE reads as [21]

$$\frac{\partial u}{\partial t} + u\frac{\partial u}{\partial x} = \nu\frac{\partial^2 u}{\partial x^2} + \eta(x,t), \tag{1}$$

where $u(x,t)$ is the velocity field; ν is viscosity; and $\eta(x,t)$ is a noise term (white in time but spatially correlated) of the form

$$\langle \hat{\eta}(k,t)\hat{\eta}(k',t')\rangle = 2D_0|k|^{\beta}\delta(k+k')\delta(t-t'),$$

where $\hat{\eta}(k,t)$ denotes the spatial Fourier transform of the noise $\eta(x,t)$ and D_0 and β are the amplitude and spectral slope of the noise. Chekhlov and Yakhot [21] showed that for $\beta = -1$ and k (or r) in the inertial range, the energy spectrum (or the second-order structure function) closely resembles the K41 predictions, i.e., $E(k) = \langle|\hat{u}(k)|^2\rangle \sim k^{-5/3}$ (or $S_2(r) \sim r^{2/3}$). However, the higher-order structure functions strongly deviate from monofractality (K41 predictions). In fact, in this case $S_{q\leq 2}(r) \sim r^{q/3}$ and $S_{q>2}(r) \sim r$. This anomalous bifractal behavior is associated with shock formation, which is an intrinsic property of the Burgers equation. Please note that the qth-order structure function $S_q(r)$ is defined as follows:

$$S_q(r) = \langle (u(x+r) - u(x))^q\rangle = \langle (\delta_r u)^q\rangle \sim r^{\zeta_q}. \tag{2}$$

The angular brackets denote spatial averaging, and r is a separation distance that varies in the inertial range. If the scaling exponent ζ_q is a nonlinear function of q, then the field is called multifractal; otherwise it is termed as monofractal [32,33].

Hayot and Jayaprakash [25–27] further generalized the results of Chekhlov and Yakhot [21,22]. Their theoretical and numerical investigations revealed that in the range $-1 < \beta < 0$, as β tends to -1, increasingly multifractal structures appear. The results of Chekhlov and Yakhot [21,22] are recovered for $\beta \leq -1$. They also showed that for $-1 < \beta < -2/3$, the scaling exponents could be analytically (with self-consistent assumptions) derived as follows:

$$\zeta_2 = -\frac{2\beta}{3}, \tag{3a}$$

$$\zeta_3 = -\beta, \tag{3b}$$

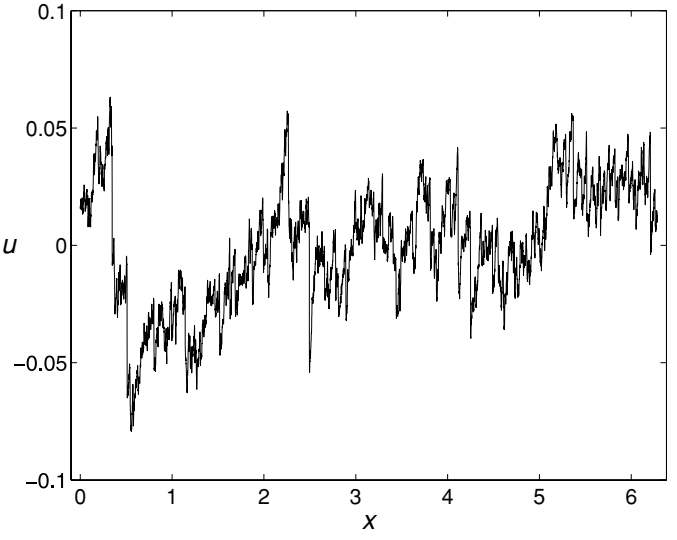

Figure 1. The velocity field $u(x,t)$ at $t = 200$ (for $\beta = -3/4$).

$$\zeta_4 = \frac{2-\beta}{3}, \tag{3c}$$

$$\zeta_5 = 1 - \frac{1+\beta}{12}. \tag{3d}$$

In this work, we selected a value of $\beta = -3/4$, which represents the case in which the dynamics of SBE portray complex multifractal behavior. Figure 1 shows a snapshot of a representative velocity field – co-existence of shocks and small-scale turbulence-like structures are clearly visible. Capturing the statistical and dynamical properties of these intricate structures could be quite challenging for any LES-SGS model, as we will see later in Section 3.

We use a Fourier collocation code to solve the SBE over a domain of length $L = 2\pi$. Time advancement is done via the explicit second-order Adams–Bashforth scheme ($\Delta t = 1 \times 10^{-4}$). The nonlinear terms are computed in the conservative form and dealiased in the Fourier domain, using the 3/2 rule; 2^{12} modes are used for the DNS ($\Delta x_{DNS} = 2\pi/8192$), whereas, 2^8 modes are used for the LES ($\Delta x_{LES} = 2\pi/512$). We would like to note that one could use lesser number of modes (say, 2^6) to perform more-or-less reliable LES of SBE. However, we found it quite challenging to estimate higher-order moments from coarser resolution runs.

The viscosity (ν) and noise amplitude (D_0) are taken to be equal to 1×10^{-5} and 1×10^{-6}, respectively. The noise term $\eta(x,t)$ is generated as follows:

$$\eta(x,t) = \sqrt{2D_0/\Delta t}\,\mathcal{F}^{-1}(|k|^{\beta/2}\hat{f}(k)), \tag{4}$$

where $\hat{f}(k)$ is the Fourier transform of a Gaussian random variable $f(x)$ with mean $= 0$ and standard deviation $= \sqrt{N}$ (such that $\langle|\hat{f}(k)|^2\rangle = 1$). The notation $\mathcal{F}^{-1}$ denotes inverse Fourier transform; N is the number of grid points (i.e., $N = 2\pi/\Delta x$). The simulations are

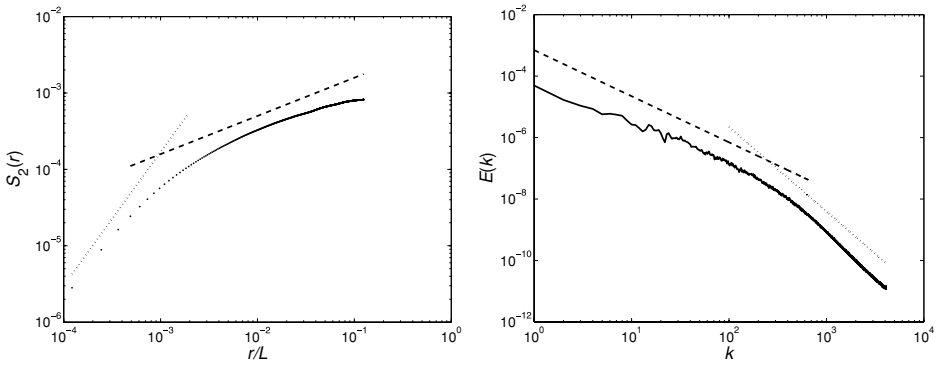

Figure 2. The second-order structure function (left) and the energy spectrum (right) of the DNS field for $\beta = -3/4$ (computed in an interval of 0.1 time units and averaged from $t = 100$ to 200). The dashed and dotted lines show theoretical predictions by Hayot and Jayaprakash [27]. The slopes of the dashed and dotted lines in the left plot are 0.50 and 1.75, respectively, whereas, the slopes of the dashed and dotted lines in the right plot are -1.50 and -2.75, respectively.

run for $T = 200$ units (i.e., 2×10^6 time steps). This corresponds to approximately two eddy turnover periods (since $\pi/u_{rms} \sim 100$). All the statistics are averaged from $t = 100$ to 200.

The second-order structure function and energy spectrum are plotted in Figure 2. In the inertial range, we get $\zeta_2 = 0.5$ as expected [see Equation (3)]. The spectral slope (σ) of -1.5 in the inertial range is also anticipated, since $\sigma = -1 - \zeta_2$. As predicted by Hayot and Jayaprakash [27], in the dissipation range, the energy spectrum portrays free-field behavior with a spectral slope of $-2 + \beta$. This, of course, leads to an exponent of 1.75 in the case of second-order structure function (see Figure 2).

In Figure 3, we have plotted the (centralized) skewness and flatness factors of the velocity increments (see p. 41 of [33] for definitions). As mentioned earlier, one of the inherent characteristics of the Burgers equation is the creation of shocks. This leads to large magnitudes of negative velocity differences, and as a consequence, the velocity increment skewnesses are always negative and increase with decreasing increment. Similarly, due to small-scale intermittency, the flatness factor increases with decreasing increment. For large increments ($r/L \to 1$), both these factors approach the Gaussian value of skewness $= 0$ and flatness $= 3$.

3. LES of the SBE

The spatially filtered version of Equation (1) is written as

$$\frac{\partial \tilde{u}}{\partial t} + \tilde{u}\frac{\partial \tilde{u}}{\partial x} = \nu \frac{\partial^2 \tilde{u}}{\partial x^2} + \tilde{\eta}(x,t) - \frac{1}{2}\frac{\partial \tau}{\partial x}, \tag{5}$$

where the tilde denotes the filtering operation, using a filter of characteristic width Δ_f. This filtered equation is now amenable for numerical solution (LES) on a grid of mesh size Δx, considerably larger than the smallest scale of motion (the Kolmogorov scale). It is common practice to use the ratio of filter width to grid spacing, $\Delta_f/\Delta x = 1$ or 2 (see Chapter 9 of [1] for detailed discussion on this ratio and its impact on error dynamics). In this study, we considered a filter to grid ratio of 1.

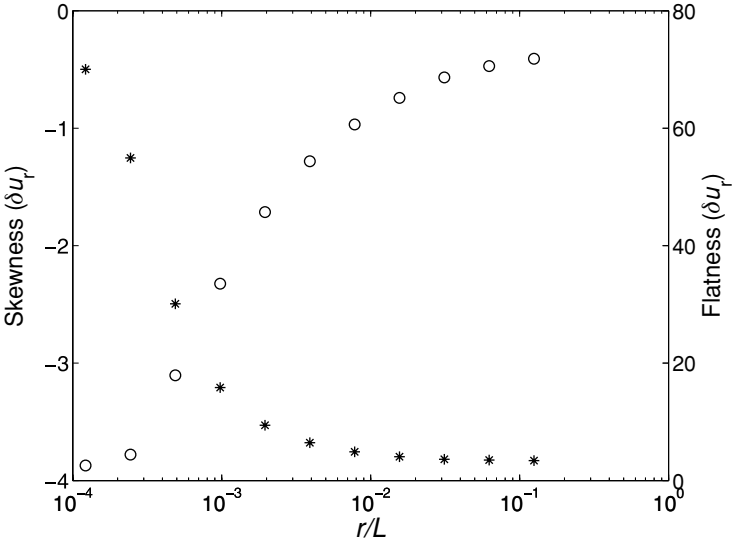

Figure 3. The skewness (circles) and flatness (stars) factors of the velocity increments as functions of r/L. These statistics are computed in an interval of 0.1 time units and averaged from $t = 100$ to 200.

The SGS stress, τ in Equation (5), defined as

$$\tau = \widetilde{u^2} - \tilde{u}\tilde{u}, \tag{6}$$

is not known. It essentially represents the contribution of unresolved scales (smaller than Δ_f) to the total momentum transport and must be parameterized (via an SGS model) as a function of the resolved velocity field. The classical Smagorinsky-type eddy-viscosity model (SMAG) expresses the SGS stress tensor in terms of the resolved strain rate tensor [34]. In the one-dimensional context, the SGS stress is of the form

$$\tau^{SMAG} = -2(C_S\Delta_f)^2 \left|\frac{\partial\tilde{u}}{\partial x}\right| \left(\frac{\partial\tilde{u}}{\partial x}\right). \tag{7}$$

This SGS model assumes that the energy dissipation rate (ϵ) equals the SGS energy production rate (P). In order to avoid this strong assumption, Wong and Lilly [35] proposed a new SGS model (henceforth denoted as WONG) based on Kolmogorov's scaling hypothesis. The one-dimensional version of this SGS model is as follows:

$$\tau^{WONG} = -2\left(C_W\Delta_f^{4/3}\right) \left(\frac{\partial\tilde{u}}{\partial x}\right). \tag{8}$$

In an LES, the SGS coefficient C_S (also known as the Smagorinsky coefficient) or C_W is usually not known and has to be specified a priori. In the case of the SBE, one could attempt to analytically derive these coefficients following the classical approach of Lilly [36] with certain assumptions. Another alternative would be to use the dynamic formulation of Germano [5, 6]. Basically, the dynamic formulation avoids the need for a priori specification of C_S or C_W because they are evaluated directly from the resolved

scales, utilizing the notion of scale similarity. The basics of the dynamic formulation have been extensively covered in Geurts [1] and Sagaut [4] and will not be reiterated here.

For the present one-dimensional case, following the error-minimization approach of Lilly [6], the dynamic SGS coefficients could be evaluated as

$$C_S^2 = \frac{\langle L_{11} M_{11} \rangle}{\langle M_{11} M_{11} \rangle}, \tag{9a}$$

$$C_W = \frac{\langle L_{11} N_{11} \rangle}{\langle N_{11} N_{11} \rangle}, \tag{9b}$$

where $L_{11} = T_{11} - \overline{\tau_{11}} = \overline{\tilde{u}^2} - \overline{\tilde{u}}\,\overline{\tilde{u}}$. This relation is known as the Germano identity. The overbar denotes test filtering at a scale $\overline{\Delta}$; τ_{11} and T_{11} are the SGS stresses at scales Δ_f and $\overline{\Delta}$, respectively. Thus, L_{11} represents the SGS stress between Δ_f and $\overline{\Delta}$. We employ a spectral cutoff filter (i.e., $\hat{F}_{\Delta_f}(k) = 1, \text{ if } k\Delta_f < \pi,$ and $\hat{F}_{\Delta_f}(k) = 0, \text{ otherwise}$), with $\overline{\Delta} = 2\Delta_f$. For this case, M_{11} and N_{11} could be written as:

$$M_{11} = -2\Delta_f^2 \left(4 \left| \overline{\frac{\partial \tilde{u}}{\partial x}} \right| \left(\overline{\frac{\partial \tilde{u}}{\partial x}} \right) - \overline{\left| \frac{\partial \tilde{u}}{\partial x} \right| \left(\frac{\partial \tilde{u}}{\partial x} \right)} \right), \tag{10a}$$

$$N_{11} = -2\Delta_f^{4/3} \overline{\frac{\partial \tilde{u}}{\partial x}} (2^{4/3} - 1). \tag{10b}$$

In Equation (9) the angular brackets denote averaging over the entire one-dimensional domain. To avoid numerical instabilities, the dynamic coefficients C_S^2 and C_W are set to zero whenever Equation (9) yields a negative value. This commonly used procedure is known as 'clipping' [1]. Qualitatively, the evolutions of the dynamic SGS coefficients are quite similar, as shown in Figure 4.

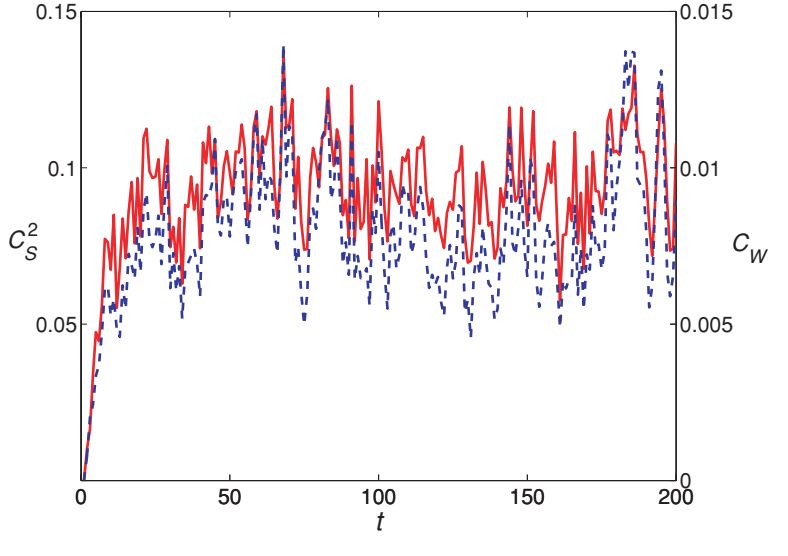

Figure 4. Evolution of the dynamic Smagorinsky coefficient (C_S^2) (red solid line) and the dynamic Wong–Lilly coefficient (C_W) (blue dashed line). The coefficients are averaged over 1 time unit interval.

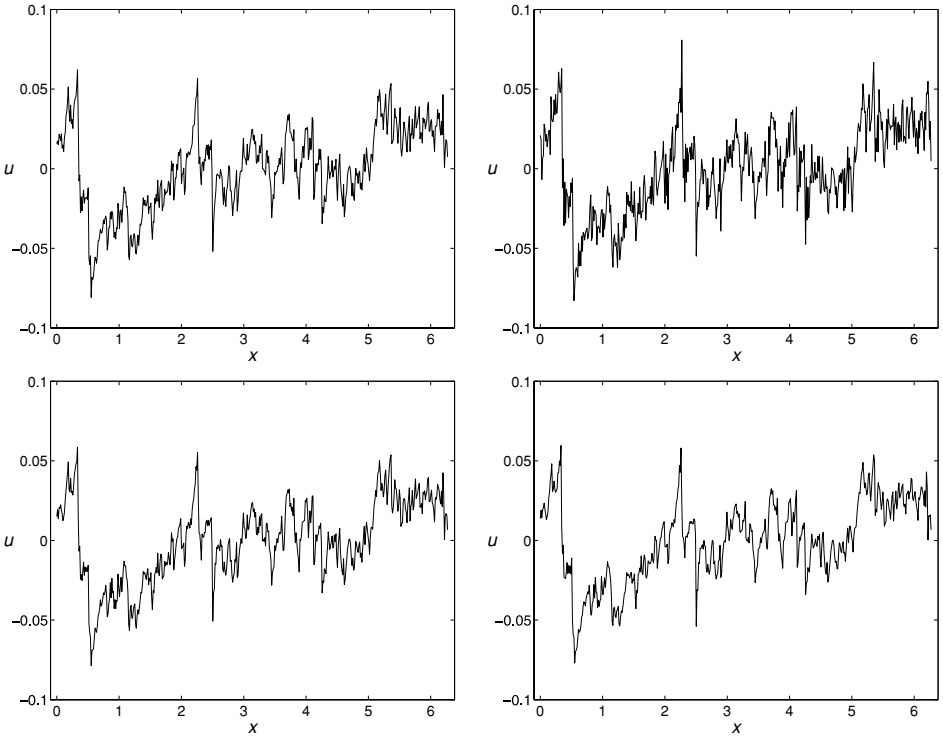

Figure 5. The coarse-grained velocity series: filtered-DNS (FDNS, top left), without any SGS model (NSGS, top right), dynamic Smagorinsky SGS model (SMAG, bottom left), and dynamic Wong–Lilly SGS model (WONG, bottom right), at $t = 200$ (for $\beta = -3/4$).

The performances of the dynamic Smagorinsky model (SMAG) and the Wong–Lilly model (WONG) are primarily assessed by comparing the simulated statistics with that of the filtered-DNS (FDNS) results. We use spectral cutoff filtering in offline mode to construct the filtered-DNS fields from the simulated DNS fields. In this case only the largest 2^8 modes are kept for comparison with LES with the same number of modes. A simulation without any SGS model (NSGS) is also performed in order to highlight the need for an SGS model in coarse-grained simulations. All the simulations start from zero-state condition, and all the LESs use identical noise forcing. The basic numerics for the LES remain the same as the DNS, as described in Section 2. In order to avoid temporal discretization error, the time step Δt is kept unchanged from the corresponding DNS value.

In Figure 5, we show snapshots of coarse-grained velocity series from all the simulations. All the series qualitatively portray the complex interaction between shocks and small scales. The simulation without any SGS model (NSGS), however, shows much higher levels of random fluctuations. This is clearer in Figure 6. The resolved-scale kinetic energy ($KE = 0.5\tilde{u}^2$) level becomes much higher for the NSGS simulation. This is due to the pileup of energy associated with the lack of SGS dissipation. This undesirable behavior becomes more discernible for LES runs, using coarser resolutions (not shown). As mentioned before, in this work we decided to use 2^8 modes to facilitate the computation of higher-order moments.

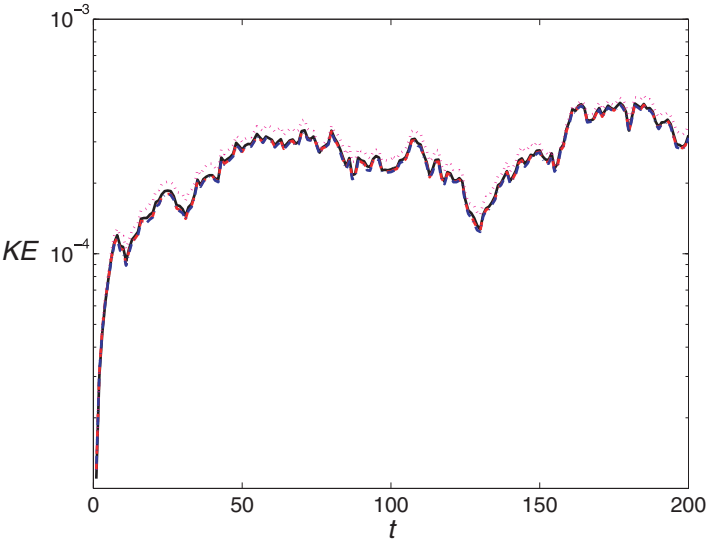

Figure 6. Evolution of kinetic energy, KE (computed every 0.1 time units and averaged over one time unit intervals). The black solid, magenta dotted, red dashed, and blue dash-dotted lines denote FDNS, NSGS, SMAG, and WONG simulations, respectively.

Next, we compare the second-order structure functions and Haar wavelet spectra from these simulations. The smoothness of wavelet spectra makes it easier to visually appraise the performance of different SGS models. Following [37], the wavelet power spectral density function $E(K_m)$ is defined as

$$E(K_m) = \frac{\langle (W^{(m)}[i])^2 \rangle \Delta x}{2\pi \ln(2)}, \tag{11}$$

where wavenumber $K_m (= 2\pi/2^m \Delta x)$ corresponds to scale $R_m (= 2^m \Delta x)$. The scale index m runs from 1 (finest scale) to $\log_2(N)$ (coarsest scale); $W^{(m)}[i]$ denotes the Haar wavelet coefficient at scale m and location i. The DNS spectra using Fourier basis (Figure 2) and wavelet basis (Figure 7) are very similar, as anticipated. The SMAG and WONG simulations follow the FDNS spectra and structure function profiles fairly well. The WONG model is, however, marginally over-dissipative. Recently, Anderson et al. [31] also reported the over-dissipation characteristic of the WONG model in the context of atmospheric boundary layer simulations. The spectra and second-order structure function corresponding to NSGS once again clearly reveal lack of energy dissipation.

In Figure 8, we compare the temporal evolution of mean SGS energy dissipation ($\langle \epsilon_{SGS} \rangle$) and mean molecular energy dissipation ($\langle \epsilon_{MOL} \rangle$). They are defined as

$$\langle \epsilon_{SGS} \rangle = -\left\langle \tau \frac{\partial \tilde{u}}{\partial x} \right\rangle, \tag{12a}$$

$$\langle \epsilon_{MOL} \rangle = \left\langle \nu \left(\frac{\partial \tilde{u}}{\partial x} \right)^2 \right\rangle. \tag{12b}$$

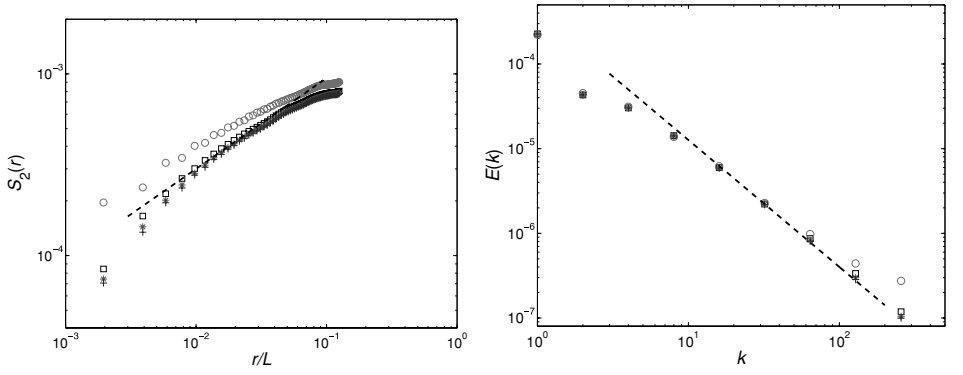

Figure 7. Second-order structure function (left) and wavelet-based energy spectra (right) computed from LES with different SGS models (computed every 0.1 time units and averaged from $t = 100$ to 200). The magenta circle, red star, and blue plus symbols denote NSGS, SMAG, and WONG simulations, respectively. The FDNS results (black square symbols) and theoretical predictions (black dashed lines) are also shown for comparison.

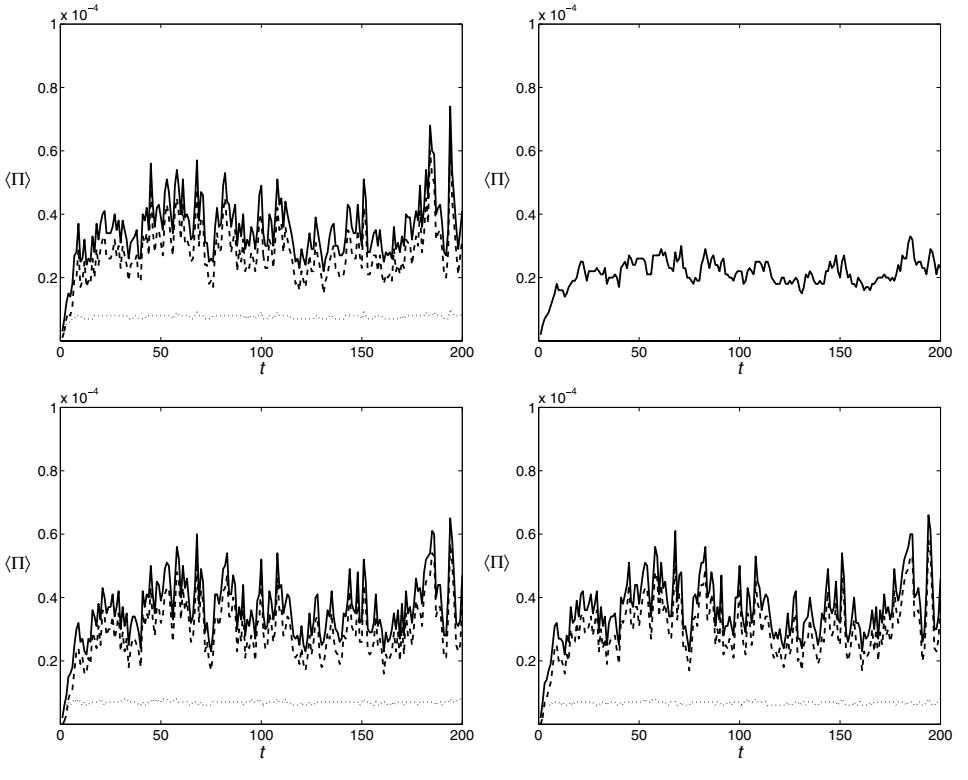

Figure 8. Comparison of temporal evolution of mean SGS ($\langle \epsilon_{SGS} \rangle$, dashed lines), molecular ($\langle \epsilon_{MOL} \rangle$, dotted lines), and total energy dissipation ($\langle \epsilon_{SGS} \rangle + \langle \epsilon_{MOL} \rangle$, solid lines): filtered DNS (FDNS, top left), without any SGS model (NSGS, top right), dynamic Smagorinsky SGS model (SMAG, bottom left), and dynamic Wong–Lilly SGS model (WONG, bottom right). These statistics are computed every 0.1 time units and averaged over 1 time unit interval.

The evolution of total energy dissipation in the cases of SMAG and WONG simulations are quite similar to the FDNS case. This corroborates the fact that these SGS models on average dissipate the right amount of energy and also reproduces the second-order statistics fairly well. Of course, there is no SGS dissipation term in the case of NSGS, and it is clear that the molecular dissipation alone is not sufficient.

An SGS model should also dissipate the right amount of resolved scale enstrophy in order to correctly model the third-order moment of velocity increments. This is a sufficient condition as shown by Meneveau [38]. The balance between the production of enstrophy ($\mathcal{P} = (\partial\tilde{u}/\partial x)^3$) and its dissipation by the SGS stress ($\mathcal{H}_{SGS} = -(\partial^3\tilde{u}/\partial x^3)\tau$) and molecular viscosity ($\mathcal{H}_{MOL} = \nu(\frac{\partial^2\tilde{u}}{\partial x^2})^2$) could be written as:

$$\left\langle \left(\frac{\partial \tilde{u}}{\partial x}\right)^3 \right\rangle = -\left\langle \frac{\partial^3 \tilde{u}}{\partial x^3}\tau \right\rangle + \left\langle \nu \left(\frac{\partial^2 \tilde{u}}{\partial x^2}\right)^2 \right\rangle. \tag{13}$$

From Figure 9, it is difficult to judge the performance of the SGS models. Both the SGS models (SMAG and WONG) as well as the FDNS more or less balance the enstrophy production and dissipation, given the assumptions made in the derivation of Equation (13) and also the uncertainty involved in the estimation of the covariances between the third-order

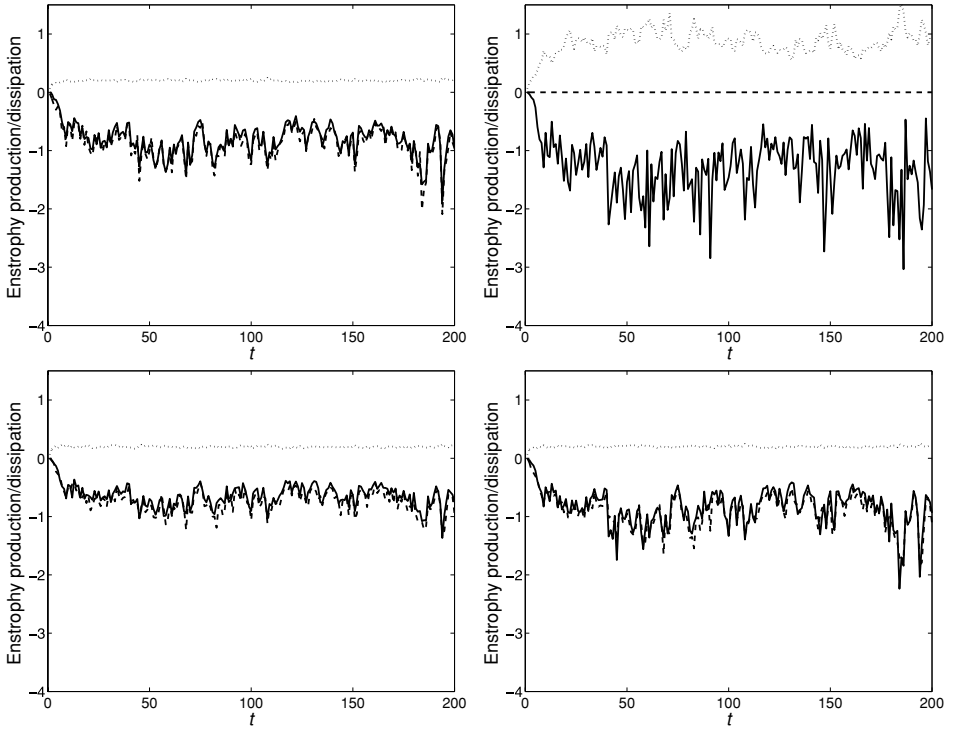

Figure 9. Comparison of temporal evolution of mean enstrophy production ($\langle\mathcal{P}\rangle$, solid lines), SGS enstrophy dissipation ($\langle\mathcal{H}_{SGS}\rangle$, dashed lines), and molecular enstrophy dissipation ($\langle\mathcal{H}_{MOL}\rangle$, dotted lines): filtered DNS (FDNS, top left), without any SGS model (NSGS, top right), dynamic Smagorinsky SGS model (SMAG, bottom left), and dynamic Wong–Lilly SGS model (WONG, bottom right). These statistics are computed every 0.1 time units and averaged over 1 time unit interval.

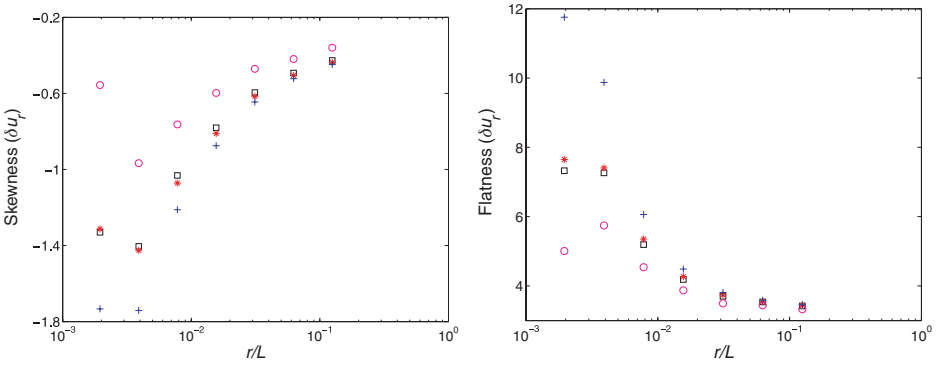

Figure 10. Skewness (left) and flatness (right) factors computed from LES with different SGS models (computed every 0.1 time units and averaged from $t = 100$ to 200). The magenta circle, red star, and blue plus symbols denote NSGS, SMAG, and WONG simulations, respectively. The FDNS results (black squares) are also shown for comparison.

derivatives and the SGS stresses. By definition, the molecular enstrophy dissipation is always positive. On the other hand, because of shock formations in the Burgers equation, the enstrophy production on average is negative. Hence, the magnitude of SGS enstrophy dissipation should be larger than the enstrophy production, which is always the case. In the case of NSGS the enstrophy balance is of course not feasible, and its consequence is reflected in the third-order statistics (see Figure 10).

From Figure 10, it is very clear that in the inertial range the dynamic Smagorinsky-model-predicted skewness and flatness factors are slightly more 'precise' than the dynamic Wong–Lilly model, when compared to the corresponding FDNS values. The NSGS case definitely does not preserve any small-scale characteristics. This implies that the inertial-range properties of Burgers turbulence are strongly dependent on the mode of SGS energy dissipation.

Next, we utilize the one-point magnitude cumulant analysis approach [39, 40] to test whether the SGS models have captured the underlying multifractality of the SBE. One-point cumulants are computed as

$$C_1(r) = \langle \ln |\delta_r u| \rangle \sim -c_1 \ln(r) \tag{14a}$$

$$C_2(r) = \langle \ln^2 |\delta_r u| \rangle - \langle \ln |\delta_r u| \rangle^2 \sim -c_2 \ln(r), \tag{14b}$$

$$C_3(r) = \langle \ln^3 |\delta_r u| \rangle - 3\langle \ln^2 |\delta_r u| \rangle \langle \ln |\delta_r u| \rangle + 2\langle \ln |\delta_r u| \rangle^3 \sim -c_3 \ln(r). \tag{14c}$$

It can be shown that the cumulant coefficients (c_n) are directly related to the scaling exponents [39–41], as follows:

$$\zeta_q = -\sum_{n=1}^{\infty} c_n \frac{q^n}{n!}. \tag{15}$$

In Figure 11, the cumulants (C_n, $n = 1$, 2, and 3^2) are plotted against r/L (please note the logarithmic abscissa scale). Interestingly, a continuous crossover is observed in the case of $C_1(r)$, as earlier reported by Delour et al. [39] in the case of various turbulent flow signals. In the present study, $C_2(r)$ and $C_3(r)$ are quite 'erratic' in contrast to Delour et al. [39]

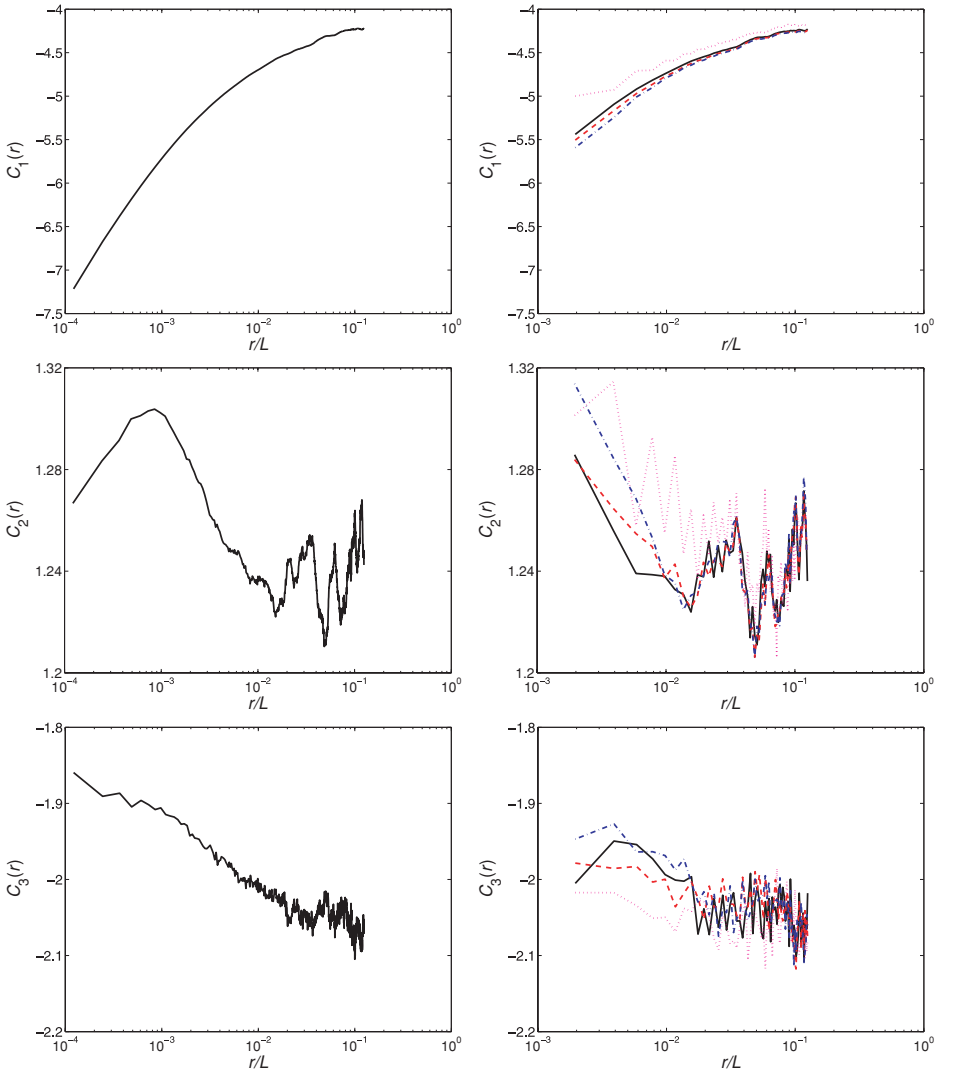

Figure 11. One-point cumulants $C_1(r)$ (top), $C_2(r)$ (middle), and $C_3(r)$ (bottom) are computed from DNS (left panel) and LES (right panel) with different SGS models (computed every 0.1 time units and averaged from $t = 100$ to 200). In the right panel, the magenta dotted, red dashed, and blue dash-dotted lines denote NSGS, SMAG, and WONG simulations, respectively. The FDNS results (black solid lines) are also shown in the right panel figures for comparison.

and Basu et al. [41]. Nevertheless, it was important to detemine if the value of ζ_2 predicted using estimated c_n and Equation (15) matched the theoretical value of $\zeta_2 = 0.5$. From DNS results (see Figure 2), it is quite clear that ζ_2 is approximately equal to 0.5 over a narrow scaling region of $7 \times 10^{-3} \leq r/L \leq 1.56 \times 10^{-2}$. We estimate the slopes of the cumulant plots over this scaling range and list them in Table 1. In the last column of Table 1, we also report $\zeta_2^{pred} = -2c_1 - 2c_2 - (\frac{8}{6})c_3$. The ζ_2^{pred} values from DNS and FDNS simulations are reasonably close to the theoretical value of $\zeta_2 = 0.5$. On the other hand, ζ_2^{pred} values from SMAG and WONG simulations are higher than 0.5. These slopes, steeper than 0.5,

Table 1. Cumulant analysis.

Simulation	c_1	c_2	c_3	ζ_2^{pred}
DNS	−0.297	0.019	0.032	0.514
FDNS	−0.316	0.021	0.035	0.544
SMAG	−0.344	0.032	0.014	0.605
WONG	−0.372	0.036	0.049	0.607

are also evident in Figure 7. Thus, our results are self-consistent. From Figure 11 and Table 1, it is also clear that the dynamic eddy-viscosity SGS models more or less capture the observed multifractality of SBE. Once more, the performance of the dynamic Smagorinsky model is found to be marginally superior than that of the dynamic Wong–Lilly model.

Recently, in the context of three-dimensional homogeneous isotropic turbulence, He et al. [42] found that the LES fields are more coherent than the DNS fields and decorrelate much more slowly. This means that the SGS have the potential to significantly modify the dynamical properties (such as predictability) of the resolved scales through nonlinear interactions. A reliable SGS modeling scheme should address this issue appropriately. He et al. [42] also speculated that in the case of Burgulence, since the velocity modes become phase-locked as shocks develop, the opposite scenario might be true (i.e., the LES fields decorrelate faster than the DNS field). In this study, we attempt to test the validity of this speculation by comparing the performance of different SGS models in simulating the temporal decorrelation property of SBE. Following He et al. [42], the normalized temporal

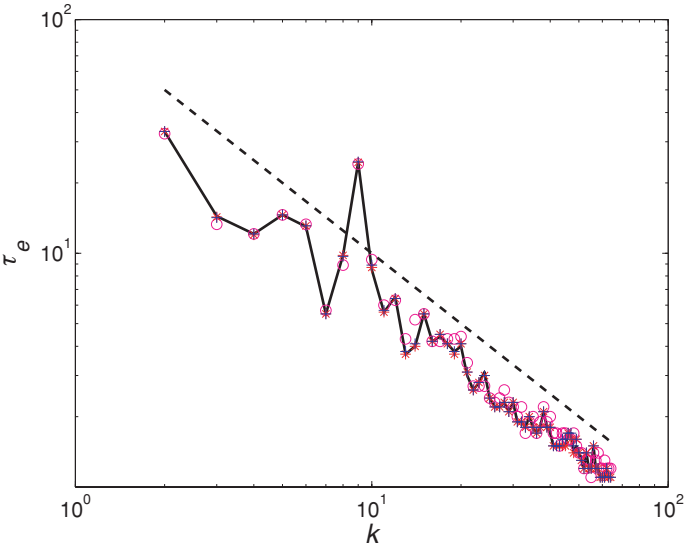

Figure 12. Decorrelation time (τ_e) of DNS and different LES models plotted against wavenumber (k). The magenta circle, red star, and blue plus symbols denote NSGS, SMAG, and WONG simulations, respectively. The black solid line represents DNS results, whereas the black dashed line represents k^{-1}.

correlation is defined as

$$C_{DNS}(k,\tau) = \frac{\langle u(k,t+\tau)u(k,t)\rangle}{\langle u(k,t)u(-k,t)\rangle}, \tag{16a}$$

$$C_{LES}(k,\tau) = \frac{\langle \tilde{u}(k,t+\tau)\tilde{u}(k,t)\rangle}{\langle \tilde{u}(k,t)\tilde{u}(-k,t)\rangle}. \tag{16b}$$

In Figure 12, we report the decorrelation time (τ_e) of the simulated fields as a function of wavenumber. Here, τ_e denotes the time lag when the normalized temporal correlation (i.e., C_{DNS} or C_{LES}) drops less than $1/e$ for a particular wavenumber. As would be intuitively expected, the larger modes have longer decorrelation times, and vice versa. The surprising behavior is the k^{-1} falloff of the temporal correlation. This behavior was also observed in He et al. [42] (where they used microscale and integral scale instead of τ_e) and could be explained by the 'sweeping hypothesis' for Eulerian time correlations [42, 43]. However, unlike He et al. [42], the coarse-grained simulations also closely follow the temporal decay behavior of the DNS; no significant faster or slower decay was observed. In other words, in this study we did not observe the plausible scenario (i.e., the LES fields being less coherent than the DNS fields) surmised by He et al. [42] to hold in the case of SBE.

4. Concluding remarks

In this study, the SBE equation which portrays multifractality is used as a toy model to explore the performance of two dynamic eddy-viscosity-type SGS models: the dynamic Smagorinsky model and the dynamic Wong–Lilly model. In terms of simulating the inertial-range properties of Burgulence, the performance of both the dynamic SGS models is satisfactory. However, the dynamic Smagorinsky model performed slightly better than the dynamic Wong–Lilly model in some cases. The simulation without any SGS model fails to preserve the essential small-scale properties. These results essentially signify that the inertial-range statistics strongly depend on the mode of SGS energy dissipation and that the dynamic eddy-viscosity-type SGS models have the potential to capture them accurately. Of course, it is not prudent to deduce generalized conclusions for the three-dimensional Navier–Stokes equations based on our study of the one-dimensional Burgers equation. The energy cascade mechanism is quite different in these two cases. With increasing computational capabilities, we might be able to perform DNS of high-Reynolds-number turbulence in the near future and revisit the intriguing issue explored in this paper.

Acknowledgements

The author is grateful to Alberto Scotti, Efi Foufoula-Georgiou, and Fernando Porté-Agel for many thought-provoking discussions. This work was partially funded by the National Science Foundation (ATM-0748606) and the Texas Advanced Research Program (003644-0003-2006) grants.

Notes

1. These SGS models are widely used by the atmospheric boundary layer turbulence community (see [31] and the references therein).
2. Estimation of C_n for $n > 3$ typically requires extremely large sample size for achieving statistical convergence, and thus is not attempted in the present study.

References

[1] B.J. Geurts, *Elements of Direct and Large-Eddy Simulation*, Edwards, Philadelphia, 2003.
[2] C. Meneveau and J. Katz, *Scale-invariance and turbulence models for large-eddy simulation*, Ann. Rev. Fluid Mech., 32 (2000), pp. 1–32.
[3] S.B. Pope, *Turbulent Flows*, Cambridge University Press, Cambridge, UK, 2000.
[4] P. Sagaut, *Large Eddy Simulation for Incompressible Flows*, Springer, Berlin, 2002.
[5] M. Germano, U. Piomelli, P. Moin, and W.H. Cabot, *A dynamic subgrid-scale eddy viscosity model*, Phys. Fluids, 3 (1991), pp. 1760–1765.
[6] D.K. Lilly, *A proposed modification of the Germano subgrid-scale closure method*, Phys. Fluids A, 4 (1992), pp. 633–635.
[7] S.B. Pope, *Ten questions concerning the large-eddy simulation of turbulent flows*, New J. Phys., 6 (2004), p. 35.
[8] J.M. Burgers, *The Nonlinear Diffusion Equation*, Reidel, Dordrecht, 1974.
[9] M.D. Love, *Subgrid modelling studies with Burgers' equation*, J. Fluid Mech., 100 (1980), p. 87.
[10] A. Scotti and C. Meneveau, *Fractal model for coarse-grained nonlinear partial differential equations*, Phys. Rev. Lett., 78 (1997), p. 867.
[11] A. Scotti and C. Meneveau, *A fractal model for large eddy simulation of turbulent flow*, Physica D, 127 (1999), p. 198.
[12] A. Das and D. Moser, *Optimal large-eddy simulation of forced Burgers equation*, Phys. Fluids, 14 (2002), pp. 4344–4351.
[13] G.D. Stefano and O.V. Vasilyev, *Sharp cutoff versus smooth filtering in large eddy simulation*, Phys. Fluids, 14 (2002), pp. 362–369.
[14] D.H. Chambers, R.J. Adrian, P. Moin, D.S. Stewart, and H.J. Sung, *Karhunen–Loéve expansion of Burgers' model of turbulence*, Phys. Fluids, 31 (1988), pp. 2573–2582.
[15] H. Choi, R. Temam, P. Moin, and J. Kim, *Feedback control for unsteady flow and its application to the stochastic Burgers equation*, J. Fluid Mech., 253 (1993), pp. 509–543.
[16] V. Yakhot and Z.-S. She, *Long-time, large-scale properties of the random-force-driven Burgers equation*, Phys. Rev. Lett., 60 (1988), pp. 1840–1843.
[17] E. Medina, T. Hwa, M. Kardar, and Y.-C. Zhang, *Burgers equation with correlated noise: renormalization-group analysis and applications to directed polymers and interface growth*, Phys. Rev. A, 39 (1989), pp. 3053–3075.
[18] Z.-S. She, E. Aurell, and U. *Frisch, The inviscid Burgers equation with initial data of Brownian type*, Comm. Math. Phys., 148 (1992), pp. 623–641.
[19] Y.G. Sinai, *Statistics of shocks in solutions of inviscid Burgers equation*, Comm. Math. Phys., 148 (1992), pp. 601–621.
[20] L. Bertini, N. Cancrini, and G. Jona-Lasinio, *The stochastic Burgers equation*, Comm. Math. Phys., 165 (1994), pp. 211–232.
[21] A. Chekhlov and V. Yakhot, *Kolmogorov turbulence in a random-force-driven Burgers equation*, Phys. Rev. E, 51 (1995), pp. R2739–R2742.
[22] A. Chekhlov and V. Yakhot, *Kolmogorov turbulence in a random-force-driven Burgers equation: Anomalous scaling and probability density functions*, Phys. Rev. E, 52 (1995), pp. 5681–5684.
[23] A.M. Polyakov, *Turbulence without pressure*, Phys. Rev. E, 52 (1995), pp. 6183–6188.
[24] V. Yakhot and A. Chekhlov, *Algebraic tails of probability density functions in the random-force-driven Burgers turbulence*, Phys. Rev. Lett., 77 (1996), p. 3118.
[25] F. Hayot and C. Jayaprakash, *Multifractality in the stochastic Burgers equation*, Phys. Rev. E, 54 (1996), pp. 4681–4684.
[26] F. Hayot and C. Jayaprakash, *Structure functions in the stochastic Burgers equation*, Phys. Rev. E, 56 (1997), pp. 227–230.
[27] F. Hayot and C. Jayaprakash, *From scaling to multiscaling in the stochastic Burgers equation*, Phys. Rev. E, 56 (1997), pp. 4259–4262.
[28] J.-P. Bouchaud and M. Mézard, *Velocity fluctuations in forced Burgers turbulence*, Phys. Rev. E, 54 (1996), pp. 5116–5121.
[29] S.A. Boldyrev, *Velocity-difference probability density functions for Burgers turbulence*, Phys. Rev. E, 55 (1997), pp. 6907–6910.
[30] R.H. Kraichnan, *Note on forced Burgers turbulence*, Phys. Fluids, 11 (1999), pp. 3738–3742.

[31] W.C. Anderson, S. Basu, and C.W. Letchford, *Comparison of dynamic subgrid-scale models for simulations of neutrally buoyant shear-driven atmospheric boundary layer flows*, Environ. Fluid Mech., 7 (2007), pp. 195–215.
[32] T. Bohr, M.H. Jensen, G. Paladin, and A. Vulpiani, *Dynamical Systems Approach to Turbulence*, Cambridge University Press, Cambridge, UK, 1998.
[33] U. Frisch, *Turbulence: The Legacy of A. N. Kolmogorov*, Cambridge University Press, Cambridge, UK, 1995.
[34] J.S. Smagorinsky, *General Circulation Experiments with the Primitive Equations*, Mon. Wea. Rev., 91 (1963), pp. 99–164.
[35] V.C. Wong and D.K. Lilly, *A comparison of two dynamic subgrid closure methods for turbulent thermal convection*, Phys. Fluids, 6 (1994), pp. 1016–1023.
[36] D.K. Lilly, *The representation of small-scale turbulence in numerical simulation experiments*, Scientific Computing Symposium on Environmental Sciences, Yorktown Heights, NY, 1967.
[37] C. Meneveau, *Analysis of turbulence in the orthonormal wavelet representation*, J. Fluid Mech., 232 (1991), pp. 469–520.
[38] C. Meneveau, *Statistics of turbulence subgrid-scale stresses: Necessary conditions and experimental results*, Phys. Fluids, 6 (1994), pp. 815–833.
[39] J. Delour, J.F. Muzy, and A. Arnéodo, *Intermittency of 1D velocity spatial profiles in turbulence: A magnitude cumulant analysis*, Eur. Phys. J. B, 23 (2001), pp. 243–248.
[40] Y. Malécot, C. Auriault, H. Kahalerras, Y. Gagne, O. Chanal, B. Chabaud, and B. Castaing, *A statistical estimator of turbulence intermittency in physical and numerical experiments*, Eur. Phys. J. B., 16 (2000), p. 549.
[41] S. Basu, E. Foufoula-Georgiou, B. Lashermes, A. Arnéodo, *Estimating intermittency exponent in neutrally stratified atmospheric surface layer flows: A robust framework based on magnitude cumulant and surrogate analyses*, Phys. Fluids, 19 (2007), p. 115102.
[42] G.-W. He, R. Rubinstein, and L.-P. Wang, *Effects of subgrid-scale modeling on time correlations in large eddy simulation*, Phys. Fluids, 14 (2002), pp. 2186–2193.
[43] Y. Kaneda, *Lagrangian and Eulerian time correlations in turbulence*, Phys. Fluids, 5 (1993), p. 2835.